nature nanotechnology

ARTICLES

PUBLISHED ONLINE: 20 FEBRUARY 2011 | DOI: 10.1038/NNANO.2011.12

Controlling protein translocation through nanopores with bio-inspired fluid walls

Erik C. Yusko[1], Jay M. Johnson[1], Sheereen Majd[1], Panchika Prangkio[1], Ryan C. Rollings[2], Jiali Li[2], Jerry Yang[3]* and Michael Mayer[1,4]*

Synthetic nanopores have been used to study individual biomolecules in high throughput, but their performance as sensors does not match that of biological ion channels. Challenges include control of nanopore diameters and surface chemistry, modification of the translocation times of single-molecule analytes through nanopores, and prevention of non-specific interactions with pore walls. Here, inspired by the olfactory sensilla of insect antennae, we show that coating nanopores with a fluid lipid bilayer tailors their surface chemistry and allows fine-tuning and dynamic variation of pore diameters in subnanometre increments. Incorporation of mobile ligands in the lipid bilayer conferred specificity and slowed the translocation of targeted proteins sufficiently to time-resolve translocation events of individual proteins. Lipid coatings also prevented pores from clogging, eliminated non-specific binding and enabled the translocation of amyloid-beta (Aβ) oligomers and fibrils. Through combined analysis of their translocation time, volume, charge, shape and ligand affinity, different proteins were identified.

Nanopores hold tremendous promise for applications such as single-molecule folding and binding assays[1–3], portable detection of (bio)warfare agents[4–6] and ultrafast sequencing of DNA or RNA[7,8]. Nanopore-based experiments provide submolecular detail on the composition of individual molecules[9] and on the formation of molecular complexes or aggregates[1,10]. All of these applications are realized through recordings of resistive current pulses during the translocation of single molecules or particles through electrolyte-filled nanopores. This Coulter counting principle makes it possible to study the size[1,4,6,11–13], conformation[14,15] and activity[16,17] of single molecules *in situ*[3,18–23]. Moreover, this technique can characterize hundreds of unlabelled single molecules per second in physiological solutions and yields distributions of measured parameters from these single-molecule investigations[3,9]. To reach the full potential of nanopore-based sensing, however, several challenges should be addressed. First, there is a need for methods that can reliably fabricate synthetic nanopores on the subnanometre scale[24] and enable controlled, dynamic variaties of pore diameters *in situ*[24,25]. Second, better control of translocation times of single-molecule analytes is required in order to achieve complete time resolution of translocation signals and more accurate determination of the amplitude and duration of resistive pulses[26–28]. Third, methods to control the surface chemistry inside synthetic pores[16] may reduce non-specific interactions of analytes with the pore walls[1,3,29] and prevent pore clogging[3]. Finally, the low frequency of translocation events at low analyte concentrations[30] and the poor specificity of the nanopores for analytes[3] need to be improved.

Nature offers a solution for most of these challenges in the design of biological nanopores[23]. Ion channel proteins, for instance, fold into three-dimensional structures with predetermined locations of individual atoms and precisely defined internal diameters that can be actuated by ligand binding or by changes in the environment of the pore[31]. Many ion channel proteins are specific towards ligands and permeants, have minimal non-specific interactions, and irreversible clogging is rare. However, the instability of these proteins and their surrounding membranes limits their application for sensing[23].

Insects detect pheromones by translocating odorant molecules through lipid-coated nanopores (diameter, 6–65 nm) that span their exoskeleton (Fig. 1a)[32–34]. These lipid coatings are thought to participate in the capture, pre-concentration and subsequent translocation of odorants to specific receptors on the dendrites of olfactory neurons in the antennae of insects[32,34]. Inspired by this design, we explored whether coating synthetic nanopores of comparable diameters with fluid lipid bilayers could provide benefits for nanopore-based, resistive pulse sensing of single proteins while addressing the associated challenges. Coating synthetic nanopores with organic molecules has been demonstrated previously, but these coatings were fixed on the surface of the pore[35–37]. Here, we introduce the concept of fluid coatings.

Advantages of fluid coatings

To create lipid-bilayer-coated nanopores (Fig. 1b), we exposed silicon chips containing a single pore through a silicon nitride window to an aqueous suspension of small unilamellar liposomes[38–41]. Spreading these liposomes on the Si_3N_4 window and on the walls of the nanopore (Supplementary Sections S1–S3) created a bilayer coating, reducing the diameter of the nanopore. The thickness and surface chemistry of this coating can be controlled accurately through the choice of lipids in the liposome preparation. For example, bilayer thickness can be fine-tuned by the length and number of double bonds of the hydrocarbon tails of the lipids (Fig. 1c), and the surface chemistry can be controlled by the nature of their polar head groups (Supplementary Section S4).

Fine-tuning of the diameter of nanopores is illustrated by the red curve in Fig. 1c. This curve resulted from a best fit of the data to a simple physical model that described the electrical resistance through the nanopore, R (Ω), as the sum of four terms: (i) the resistance of the cylindrical nanopore, (ii) the access resistance to and from the nanopore[31], (iii) the resistance of the cylindrical channel

[1]Department of Biomedical Engineering, University of Michigan, Ann Arbor, Michigan 48109, USA, [2]Department of Physics, University of Arkansas, Fayetteville, Arkansas 72701, USA, [3]Department of Chemistry and Biochemistry, University of California, San Diego, California 92093, USA, [4]Department of Chemical Engineering, University of Michigan, Ann Arbor, Michigan 48109, USA. *e-mail: jerryyang@ucsd.edu; mimayer@umich.edu

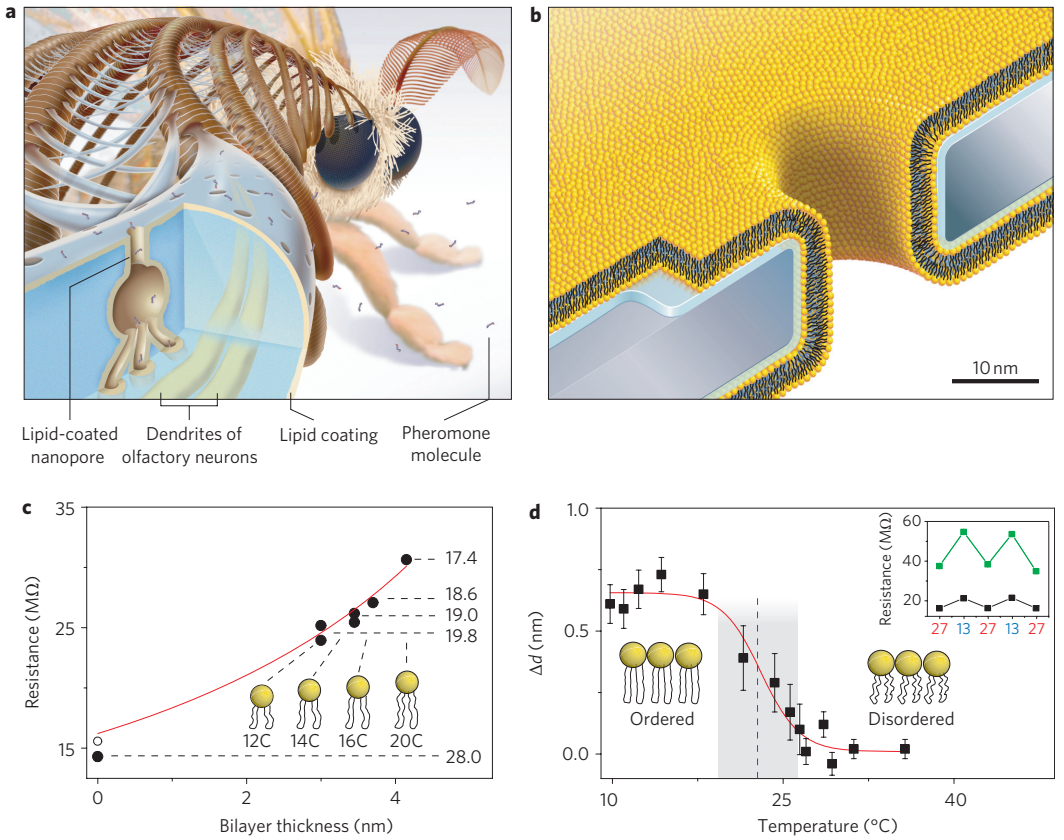

Figure 1 | Bio-inspired synthetic nanopores with bilayer-coated fluid walls. a, Drawing showing a cross-section through one sensillum in the antenna of the silk moth *Bombyx mori*. Capture, pre-concentration, and translocation of pheromones through the exoskeleton of these sensilla towards dendrites of olfactory neurons is thought to occur via lipid-coated nanopores[32–34]. **b**, Drawing, to scale, showing a synthetic, lipid-coated (yellow) nanopore in a silicon nitride substrate (grey) and the interstitial water layer (blue). **c**, Nanopore resistance and corresponding open pore diameter (indicated to the right of the curve, in nm) as a function of the thickness of the bilayer coating[59]. The red curve is a best fit of the data to equation (1). Numbers underneath the lipid schematics refer to the number of carbons in their acyl chains (Table 1). **d**, Actuation of nanopore diameters by a change in the thickness of the bilayer coating, Δd, in response to a thermal phase transition of DMPC lipids (Supplementary Section S1). The blue dotted line and grey shaded region represent the mean value and range of phase transition temperatures reported for DMPC lipids[44]. Inset: cycling the temperature between 13 °C and 27 °C varied the pore diameter dynamically, as indicated by the larger changes in electrical resistance through a pore with a bilayer (green squares) than without a bilayer (black squares).

through the silicon nitride window leading to the pore (see Supplementary Section S1 for a schematic drawing), and (iv) the access resistance to this cylindrical channel. These four series resistances are represented in sequence by the terms in equation (1) (see Supplementary Section S1 for a derivation):

$$R = \frac{\rho(l_P + 2d + 2w_L)}{\pi(r_P - d - w_L)^2} + \frac{\rho}{2(r_P - d - w_L)} + \frac{\rho(l_C + 2d + 2w_L)}{\pi(r_C - d - w_L)^2} + \frac{\rho}{4(r_C - d - w_L)} \quad (1)$$

where ρ (Ω m) represents the resistivity of the electrolyte, l_P (m) the length of the cylindrical nanopore, d (m) the thickness of the lipid bilayer (Table 1), w_L (m) the thickness of the interstitial water layer between the bilayer and the silicon nitride wall of the pore[42,43], r_P (m) the radius of the nanopore, l_C (m) the length of the cylindrical channel through the silicon nitride leading to the pore, and r_C (m) the radius of this cylindrical channel (see Supplementary Section S1 for the values of ρ, l_P, r_P, l_C and r_C).

Equation (1) shows that this model estimates the effective, open radius of a pore by taking into account the reduction of its radius and increase of its length as a function of the thickness of the bilayer coating and the thickness of the interstitial water layer

Table 1 | Lipids used in this work to coat nanopore walls.

Chemical name	Abbreviation	Acyl chains*	Bilayer thickness† (nm)
1,2-dilauroyl-*sn*-glycero-3-phosphocholine	DLPC	(12:0)	3.0±0.1
1,2-dimyristoyl-*sn*-glycero-3-phosphocholine	DMPC	(14:0)	3.4±0.1
1,2-dipalmitoleoyl-*sn*-glycero-3-phosphocholine	DΔPPC	(16:1)	3.6±0.1
1,2-dieicosenoyl-*sn*-glycero-3-phosphocholine	DEPC	(20:1)	4.2±0.1
1-palmitoyl-2-oleoyl-*sn*-glycero-3-phosphocholine	POPC	(18:1–16:0)	3.7±0.1
1,2-dipalmitoyl-*sn*-glycero-3-phosphoethanolamine-*N*-(cap biotinyl)	Biotin-PE	(16:0)	—

*For lipids with two identical acyl chains, (c:db) indicates the number of carbons (c) and the number of double bonds (db); for lipids with two different acyl chains, (c1:db1–c2:db2) refer to acyl chains 1 and 2.
†Thickness according to ref. 59.

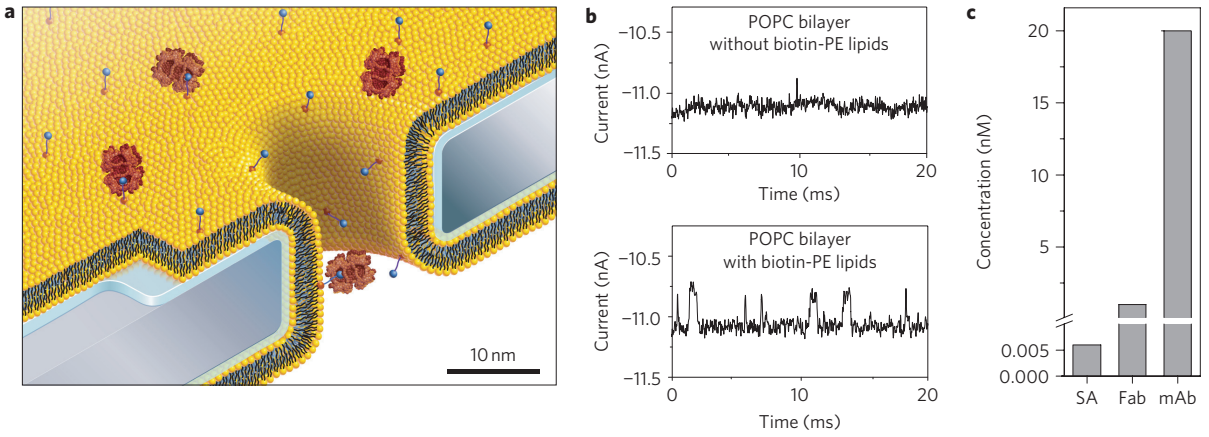

Figure 2 | Capture, affinity-dependent pre-concentration and translocation of specific proteins after binding to ligands on mobile lipid anchors. a, Drawing, to scale, illustrating binding of streptavidin (large red) to specific lipid-anchored biotin-PE (blue circles) followed by single-molecule translocation of the anchored complex through the nanopore. **b**, Current versus time traces illustrating capture, pre-concentration and reduced translocation speed of streptavidin. In the absence of biotin groups, only rare translocation events with short translocation times, t_d, could be detected in electrolytes containing 6 pM streptavidin (top current trace). In contrast, 0.4 mol% of biotinylated lipids in the lipid coating strongly increased the event frequency and slowed down the translocation speed sufficiently to enable complete time resolution of translocation events (bottom current trace). **c**, Minimum bulk concentrations of streptavidin (SA), polyclonal anti-biotin Fab fragments (Fab) and monoclonal anti-biotin IgG antibodies (mAb) required to observe at least 30–100 translocation events per second.

between the bilayer and the silicon nitride wall of the pore. A fit of the data in Fig. 1c to this model returned a thickness of the water layer of $w_L = 1.2 \pm 0.1$ nm (literature values, 0.5–1.7 nm)[42,43] as the only fitting parameter. The excellent fit of the data to equation (1) ($R^2 = 0.97$, $N = 7$) and the realistic value for the thickness of the water layer suggest that self-assembled bilayer coatings make it possible to fine-tune and predict the radius of a cylindrical nanopore in increments of two carbon atoms (albeit in a range limited to lipids that can generate stable supported lipid bilayers).

Because the sensitivity and information content of nanopore-based single-molecule experiments depend strongly on the size of the pore, one particularly desirable feature for nanopore sensing would be the ability to adjust the diameter of a nanopore dynamically to the size of various analytes, *in situ*. Figure 1d demonstrates that a thermal phase transition of a coating of DMPC lipids (Table 1) from the ordered gel phase (L_β) to the disordered liquid-crystalline phase (L_α) decreased the estimated thickness of the bilayer coating by $\Delta d \approx 0.7$ nm (literature values, 0.9–1.1 nm)[44–46], and made it possible to vary the diameter of the nanopores dynamically by 1.4 ± 0.1 nm. Figure 1d also shows that the midpoint (dashed blue line) and range (grey area) of the phase transition in the nanopore coating occurred precisely at the temperature previously reported for DMPC lipids of 23.5 ± 2.3 °C (ref. 44). Changing the diameter of nanopores by a phase transition of lipids may be a relevant mechanism by which insects regulate their water uptake and evaporative loss through lipid-coated nanopores in their exoskeleton[34,47]. In the context of synthetic nanopores, this bio-inspired capability of changing pore diameters constitutes a novel approach to determine thermal phase transition temperatures of lipid bilayers, *in situ*.

In addition to fine-tuning and dynamically varying the diameters of nanopores, bilayer coatings provide a straightforward strategy to render nanopore recordings specific for certain analytes by functionalizing the bilayer surface with ligands or receptors. Figure 2 illustrates that adding defined mole fractions of lipids with desired functional groups (here, biotinylated lipids) during the formulation of liposomes and the subsequent formation of a bilayer coating[40] can control the surface density of ligands in and around the pore. These lipid-anchored ligands, which were mobile within the fluid sheet of the lipid bilayer, could concentrate dilute analytes from the bulk solution to specific ligands on the bilayer surface and deliver these analytes to the pore by two-dimensional diffusion (Fig. 2a,b). This same basic principle is thought to occur on the lipid coating of olfactory sensilla in insect antennae, contributing to the extremely sensitive detection of lipophilic pheromones by insects[32,34,48].

Pre-concentrating and translocating analytes that are bound to a fluid surface also made it possible to distinguish between different analytes based on their affinity to the displayed ligand (Fig. 2c). For instance, proteins present at picomolar concentrations in the bulk electrolyte solution concentrated at the surface and induced frequent translocation events if they bound with high affinity to lipid-anchored ligands in the bilayer. In contrast, proteins with a low affinity to these ligands required more than a 300-fold increase in bulk concentration to reach comparable frequencies of time-resolved translocation events (Fig. 2c). In the case of streptavidin, polyclonal anti-biotin Fab fragments and monoclonal anti-biotin IgG antibodies, we found that to reach a frequency of 30–100 translocation events per second, a concentration of only 0.006 nM streptavidin was required, compared to 1 nM of Fab fragment and 20 nM monoclonal antibody. Control experiments revealed that in the absence of biotinylated lipids in the bilayer coating, or in the presence of excess biotin in solution, the frequency of detectable translocation events for each protein was up to 500-fold lower than in the presence of specific capture sites in the bilayer (Fig. 2b and Supplementary Section S5).

Lipid coating resolves translocation events

The capability of moving captured analytes through pores with fluid walls made it possible to obtain a translocation time t_d through the pore, as well as the corresponding amplitude of the resistive pulses, ΔI. This information is unique to the fluid nanopore coatings introduced here; previous reports on nanopore recordings with specific, surface-attached binding groups captured analytes at permanently fixed positions[4,5] and could therefore not allow translocation of bound analytes, thereby excluding the possibility of determining t_d or relating ΔI to the molecular volume of the bound analyte. An additional benefit of translocating analytes bound to a lipid anchor emerges in situations where the intrinsic translocation speed of the unbound analyte through a pore is too fast to resolve

t_d and ΔI completely in time, a problem encountered previously by other groups[26–28].

Figure 2b and Supplementary Section S5 show that translocation events of individual proteins could not be fully resolved without lipid-anchored capture sites. Anchoring analytes to lipids during their passage through the pore has the advantage that the translocation speed is dominated by the high viscosity of the bilayer coating rather than the low viscosity of the aqueous electrolyte in the pore[49]. The resulting prolonged translocation times enable time-resolved detection of t_d (Fig. 3) and ΔI (Fig. 4), combined with accurate, quantitative characterization of individual proteins. Alternative strategies for prolonging the translocation time by increasing the length of the pore or the viscosity of the electrolyte, or by reducing the applied voltage, have been associated with a reduction in the amplitude of translocation events and have reduced the signal-to-noise ratio[28]. In contrast, bilayer coatings with fluid capture sites can fine-tune the viscosity of the bilayer and prolong the translocation times of lipid-anchored analytes, while keeping the conductivity of the aqueous electrolyte the same.

Figure 3a demonstrates that acyl chains with increasing length and saturation can slow down translocation speeds. For instance, POPC lipids with one monounsaturated acyl chain of 18 carbon atoms and a second saturated acyl chain of 16 carbons generated ~1.4 times more viscous bilayers than DΔPPC lipids with two monounsaturated acyl chains of 16 carbons. For streptavidin, the most frequently observed translocation times using these two bilayer coatings were 114 ± 15 μs with the POPC coating and 81 ± 10 μs with the DΔPPC coating (Fig. 3a). Translocation speeds could be slowed down even further by adding 50 mol% cholesterol to a POPC bilayer; in this case the most frequently observed translocation time of Fab fragments doubled from 78 ± 5 μs to 175 ± 4 μs (Fig. 3b).

Complete time resolution of translocation events of lipid-anchored proteins allowed us to determine the volume of individual translocating proteins based on the accurate acquisition of the amplitude of resistive pulses, $\Delta I(t)$. Figure 4 shows the amplitude distributions of the resistive pulses for three different biotin-binding proteins. We used equation (2) to estimate the transiently excluded volume of electrolyte, $\Lambda(t)$ (m^3) during the translocation of these three proteins[12,13,50]:

$$\Delta I(t) = \frac{\gamma V_a \Lambda(t)}{\rho (l_P + 1.6 r_P)^2} S\left(\frac{r_P}{d_M}\right) \quad (2)$$

In this equation, γ (unitless) represents a shape factor[51] with a value of 1.5 for spheres, V_a (V) is the total applied voltage, and $S(r_P/d_M)$ is a correction factor that depends on the relative values of r_P and the diameter of the molecule, d_M. Like most groups, we used a value of 1 for $S(r_P, d_M)$ for all calculations[12,13]. Because $\Lambda(t)$ from the translocation of spheroidal particles is approximately equal to the molecular volume of the particles[14,29], we were able to estimate the molecular volumes of streptavidin (94 ± 18 nm^3; literature value, 105 ± 3 nm^3)[52], Fab fragments (172 ± 31 nm^3; literature value, ~140 nm^3)[53] and antibodies (308–696 nm^3; literature value, 347 ± 15 nm^3)[54]. The distributions of ΔI values for streptavidin (Fig. 4a) and Fab fragments (Fig. 4b) were significantly narrower than the distribution for the antibodies (Fig. 4c). Because control experiments revealed that the broad distribution was not caused by contamination of the antibody sample with other proteins (Supplementary Section S6), we attribute the broad distribution of ΔI values in Fig. 4c primarily to the complex molecular shape of IgG antibodies ($\gamma \neq 1.5$) compared to the approximately spherical shape ($\gamma \approx 1.5$) of streptavidin and Fab fragments (for a detailed discussion on the proposed effect of molecular shape on ΔI, see Supplementary Section S6).

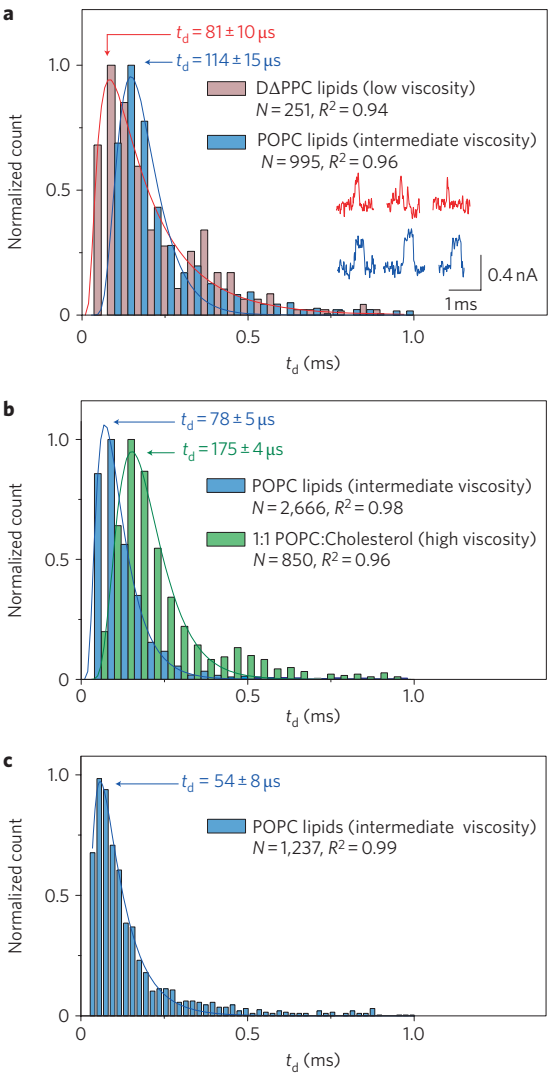

Figure 3 | Controlling the translocation times, t_d, of single lipid-anchored proteins by the viscosity of the bilayer coating and distinguishing proteins by their most probable t_d values. a, Distribution of translocation times of streptavidin. Insets: current versus time traces illustrating that t_d could be prolonged more with intermediate-viscosity POPC bilayers (blue current traces) than with low-viscosity DΔPPC bilayers (red current traces). **b**, Translocation of anti-biotin Fab fragments through nanopores with bilayers of intermediate viscosity (POPC) or high viscosity (~49 mol% cholesterol and 50 mol% POPC). **c**, Translocation of anti-biotin antibodies through a pore with a coating of intermediate viscosity (POPC). Red, blue and green curves represent a best fit of the corresponding data to a biased diffusion first passage time model[14] (equation (S10) in Supplementary Section S5). All bilayers contained 0.15–0.4 mol% biotin-PE. See Supplementary Sections S7 and S9 for binning methods, errors of t_d and measurement errors.

Determining translocation time and charge of proteins

Figure 3 shows that different proteins moved through the nanopores at different distributed speeds, as expected for biased diffusion first passage time processes[14]. Because we performed the experiments with streptavidin using a different pore (see Supplementary Table S1 for the dimensions of the pores used for all experiments), a direct comparison of the most frequently observed t_d values was only possible between Fab fragments (78 ± 5 μs, blue bars in Fig. 3b) and monoclonal antibodies (54 ± 8 μs; Fig. 3c). The observed differences in t_d values added a third dimension for distinguishing between different proteins in addition to comparing

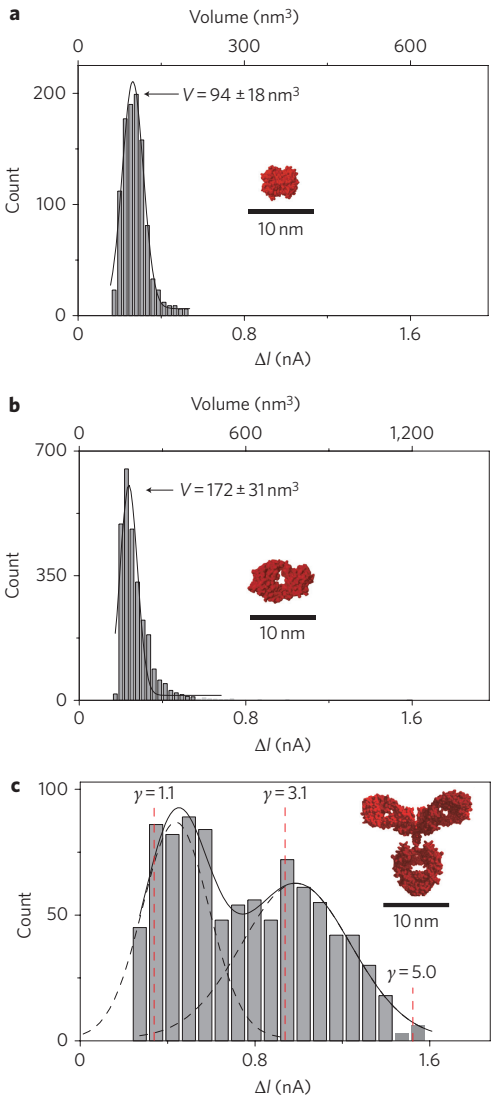

Figure 4 | Distribution of ΔI values and corresponding molecular volumes and shape factors of individual proteins translocating through bilayer-coated nanopores with biotinylated lipids. a–c, Translocation of streptavidin (**a**), anti-biotin Fab fragments (**b**) and anti-biotin antibodies (**c**); dashed red lines indicate ΔI values that would be expected for IgG antibodies with a volume of 347 nm^3 and different shape factors γ (see Supplementary Section S6 for a schematic illustration and discussion of shape factors)[51,54].

their affinity to specific ligands based on the frequency of translocation events (Fig. 2c) and quantifying their molecular volumes based on ΔI values (Fig. 4a–c).

Because the translocation speeds of different lipid-anchored proteins varied, we hypothesized that the fluid nature of the pore walls may minimize non-specific adsorption processes and open the door to determining the net charge of proteins. To test this hypothesis, we developed the simplest possible model to yield a relationship between t_d of a lipid-anchored protein and the net charge of this protein, $|z| \times e$, based on a model introduced recently by Sexton and colleagues[26]. Here z (unitless) is the net valency of the overall charge on the protein and e (C) is the elementary charge of an electron. This model assumes that a charged protein experiences an electrophoretic force that is opposed by the viscous drag inside the pore, leading to a constant drift velocity (l_P/t_d) through the pore. It also assumes that the viscous drag of lipid-anchored proteins is determined by the diffusion constant of the lipid anchor, D_L (m^2 s^{-1}), in the lipid bilayer, rather than by the diffusion

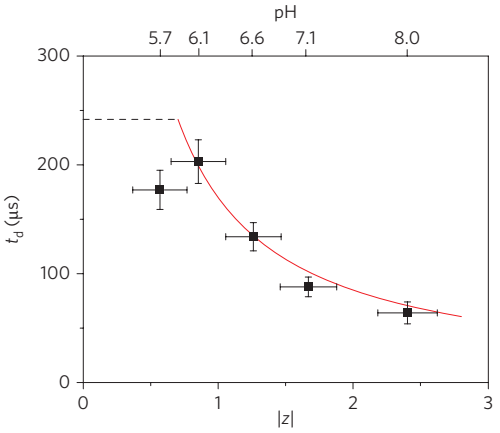

Figure 5 | Comparison of experimental and theoretical values of charge-dependent translocation times of streptavidin. Experimental values are shown in black squares and the red curve represents the theoretical prediction by equation (3). Dashed black line corresponds to the expected translocation time for streptavidin assuming a translocation event due purely to diffusion in one dimension without an electrophoretic effect that is, $t_d = \langle I_P \rangle^2 / (2D_L)$. The valence |z| of the net charge of streptavidin was varied by the pH of the electrolyte[55]. The length of the pore with the bilayer coating was 28 ± 0.2 nm. Note that the red curve is not a best fit to the data; it is the prediction of t_d as a function of |z| according to equation (3) when all parameters were fixed to their known values.

constant of the protein in the aqueous electrolyte inside the pore lumen[49]. Based on these assumptions, we derived equation (3) to predict t_d values theoretically (for a detailed derivation and additional assumptions, see Supplementary Section S8):

$$t_d = \frac{l_P^2 \, k_B T}{|z| \, e \, V_P \, D_L} \qquad (3)$$

where k_B (J K^{-1}) is the Boltzmann constant, T (K) is temperature and V_P (V) refers to the part of the total applied voltage that drops inside the pore; it does not include the voltage drop due to the access resistance to and from the pore (Supplementary Section S8).

Equation (3) made it possible to compare theoretically predicted t_d values with experimentally determined values for proteins with known net charge. Figure 5 shows this comparison for translocation events of streptavidin at five different pH values in the recording electrolyte and therefore five different values of |z|. The excellent agreement between the data (black squares) and the predicted t_d values (red curve) supports the simple model used for the derivation of equation (3).

Table 2 | Comparison of diffusion coefficients of lipid-anchored proteins within the nanopore, D_P, with diffusion coefficients of lipids, D_L, in coatings of two different lipid bilayers on three different nanopores.

Protein	Lipid bilayer*	$D_L^{\dagger}$ (nm^2 μs^{-1})	$D_P^{\ddagger}$ (nm^2 μs^{-1})	ΔD (%)
SA[§]	DΔPPC	1.56 ± 0.16	1.7 ± 0.4	+9
SA[§]	POPC	1.13 ± 0.11	1.2 ± 0.3	+6
SA[‖]	POPC	1.65 ± 0.17	1.9 ± 0.5	+15
mAb[¶]	POPC	1.29 ± 0.13	2.6 ± 0.7	+100
Fab[¶]	POPC	1.27 ± 0.13	1.5 ± 0.2	+18

*All lipid bilayers also contained 0.15–0.4 mol% biotin-PE. †Values for D_L were determined by FRAP as described in Supplementary Section S2. ‡Values for D_P were determined with equation (3) based on the most frequently measured values of t_d and values of |z| for streptavidin from ref. 55 and values of |z| for mAb and Fab as determined by capillary electrophoresis (Supplementary Section S8). §Nanopore dimensions: $r_P = 9.6$ nm, $l_P = 18$ nm. ‖Nanopore dimensions: $r_P = 10.5$ nm, $l_P = 18$ nm. ¶Nanopore dimensions: $r_P = 16.5$ nm, $l_P = 22$ nm.

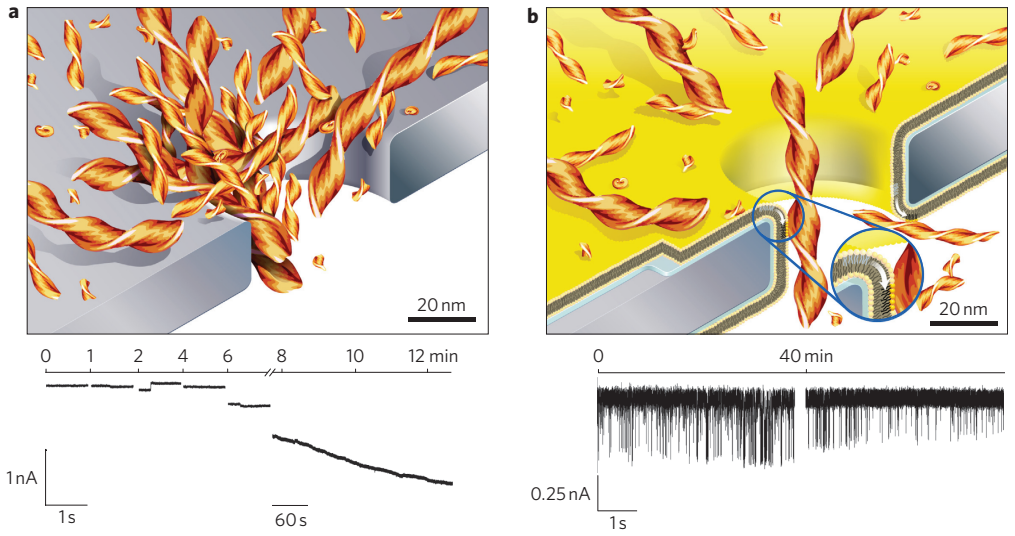

Figure 6 | Bilayer-coated nanopores resist clogging and enable monitoring of the aggregation of Aβ peptides. a, Representation of clogging of uncoated nanopores and a typical current versus time trace during clogging of a nanopore by Aβ aggregates. This concatenated current trace shows several 1 s recordings and one 5 min recording. **b**, Representation of translocation of individual Aβ aggregates through a bilayer-coated nanopore with a fluid wall (white arrow in the inset) and a typical current versus time trace of translocation events. The bilayer coating confers non-fouling properties to these pores and enables resistive pulse recordings over at least 40 min without clogging. Both recordings are 5 s long; one was taken immediately after addition of the Aβ sample and the other, 40 min later. Aβ (1–40) samples were aggregated for 72 h.

Additional support for this model comes from a comparison between two bilayer coatings of different viscosity. In one experiment we coated the nanopore with a POPC bilayer and in the other experiment with a DΔPPC bilayer. Before adding streptavidin to the top compartment of the chips, we determined the lateral diffusion coefficient of lipids in the POPC bilayer ($D_L = 1.13 \pm 0.11$ nm^2 μs^{-1}) and in the DΔPPC bilayer ($D_L = 1.56 \pm 0.16$ nm^2 μs^{-1}) by fluorescence recovery after photobleaching (FRAP) experiments on the silicon nitride support (Supplementary Section S2)[57]. With these D_L values and a valence of net charge of $|z| = |-1.9 \pm 0.4|$ at pH 7.4 (ref. 55), equation (3) predicted a translocation time for streptavidin of 126 ± 29 μs in POPC-coated pores and of 91 ± 21 μs in DΔPPC-coated pores. Experimentally, the most frequently observed translocation time of streptavidin (Fig. 3a) was 114 ± 15 μs through pores with a POPC coating (deviation from the predicted value, −10%) and 81 ± 10 μs through pores with a DΔPPC coating (deviation from the predicted value, −11%). Taken together with the data in Table 2, the excellent agreement between the theoretically predicted values of t_d and the experimentally measured t_d values confirm that translocation times of lipid-anchored analytes were indeed dominated by the viscosity of the bilayer[49] and were, hence, insensitive to the shape of the proteins (Fig. 3b,c).

These observations suggest the possibility of using t_d values, in analogy to migration times in electrophoresis, to distinguish between and possibly identify specific proteins. The agreement between theory and experiment also suggests that determining translocation times of lipid-anchored proteins through a bilayer-coated nanopore makes it possible to determine the net charge of proteins. For instance, at pH 7.4, the measured t_d values suggest a net charge between −2.9 and −5.3 for the polyclonal anti-biotin Fab fragments and a net charge of -4.2 ± 0.5 for the monoclonal anti-biotin antibodies (Supplementary Section S8). These values agree well with results from capillary electrophoresis experiments (Supplementary Section S8). Moreover, for a protein with known charge, translocation experiments combined with equation (3) make it possible to determine—non-optically—the lateral diffusion constants of lipids and therefore the fluidity of bilayers, within seconds (Table 2). This attribute might be useful in testing therapeutic compounds for their propensity to change membrane fluidity[56].

Finally, the agreement between predicted and experimental t_d values suggests that the measured t_d values are close to the 'true' electrophoretic translocation times. In other words, these measured translocation times represent translocation in the absence of non-specific adsorption of proteins to the bilayer coating or to the silicon nitride substrates. This point is important, because the t_d values from all single-molecule translocation experiments with proteins reported to date have been affected by non-specific adsorption of the proteins to the nanopore walls[1,14,26]. In some cases, these interactions increased the translocation times of proteins by several orders of magnitude[26].

Aggregated Aβ peptides translocate without clogging

Owing to the unique capability of fluid bilayer coatings to eliminate non-specific interactions, these pores made it possible to analyse translocation events of molecules that aggregate and have a tendency to clog nanopores. Amyloidogenic peptides, such as Alzheimer's disease-related amyloid-beta (Aβ) peptides[57], belong to this category of molecules. The current versus time trace in Fig. 6a shows that a nanopore without a bilayer coating clogged within minutes after addition of Aβ peptides. Despite several attempts, we were never able to detect translocation events from samples of Aβ peptides using uncoated pores. In contrast, Fig. 6b illustrates that coating nanopores with bio-inspired, fluid lipid bilayers introduced non-fouling properties to these pores and made it possible to detect numerous large-amplitude translocation events due to the passage of individual Aβ oligomers and fibrils.

Conclusions

In conclusion, the crucial novelty of lipid-coated, synthetic nanopores lies in the multifunctional and fluid nature of the self-assembled coating. This singular, bio-inspired strategy addresses many of the unmet challenges in nanopore sensing and is particularly beneficial in the context of single-molecule studies of native proteins. For example, the fluidity of the coating enables the capture and concentration of proteins from dilute solutions and permits translocation of lipid-anchored proteins at frequencies that reveal information about their affinity to ligands on these lipid anchors. Fluid coatings also eliminate non-specific adsorption

of proteins to the synthetic walls of the pore by translocating captured proteins on top of a fluid, biocompatible lipid bilayer and establish a predictable, quantitative relationship between translocation times and the charge of individual proteins. The viscous character of the fluid coating slows the translocation speed of lipid-anchored proteins and makes it possible to introduce selectivity while completely resolving translocation events in time. These viscous coatings therefore enable accurate quantitative analyses of molecular volume and qualitative analyses of the shape of individual proteins. The anti-fouling character of fluid coatings made it possible to translocate aggregated forms of disease-relevant Aβ peptides through the pore without clogging. This capability may open the door to analyses of diameter, length and volume in a large number of individual Aβ oligomers and fibrils during their aggregation *in situ*.

Methods

Lipids and proteins. All phospholipids were obtained from Avanti Polar Lipids. Streptavidin and monoclonal anti-biotin antibody (mAb, B7653) were purchased from Sigma Aldrich and polyclonal anti-biotin Fab fragments (Fab, 20938) from Rockland.

Nanopores. A focused ion beam was used to fabricate nanopores in a silicon nitride membrane that was supported by a silicon chip (see Supplementary Section S1 for information on the pores)[58]. Before the experiments, the pore-containing chips were cleaned for at least 30 min with a fresh mixture of 3:1 (v/v) concentrated sulphuric acid and 30% (v/v) aqueous hydrogen peroxide solution at 60–70 °C, followed by rinsing with deionized water and drying with argon gas. To create separate fluid compartments on either side of the nanopore, the chip was mounted between two pieces of cured polydimethylsiloxane (PDMS)[10]. After each experiment, the silicon chips were rinsed for 2–3 min successively with the following solvents: water, ethanol, methanol and chloroform. The chips were stored in chloroform between experiments.

Formation of supported lipid bilayers. Supported lipid bilayers were formed by the fusion of small unilamellar vesicles (SUVs)[38–41]. These SUVs were prepared as described in Supplementary Section S2. To form the supported lipid bilayer on silicon nitride membranes, we filled the top compartment of the PDMS fluidic setup with 10–30 μl of the aqueous solution with the SUVs and the bottom compartment with a 150 mM KCl solution without liposomes. After 5–10 min, excess SUVs were removed by immersing the entire fluidic setup for 5–10 min in a large (500 ml) beaker containing deionized water. Before recordings, the fluidic compartments were filled with the desired electrolyte. Each liposome preparation contained 0.8 mol% of the fluorescently labelled lipid, 1,2-dipalmitoyl-*sn*-glycero-3-phosphoethanolamine-*N*-(lissamine rhodamine B sulphonyl) (Rh-PE) for measuring the fluidity of lipid bilayers by FRAP (Supplementary Section S2).

Electrical resistance as a function of bilayer thickness. We used Ag/AgCl pellet electrodes (Warner Instruments) to monitor ionic currents through electrolyte-filled nanopores with a patch-clamp amplifier (Axopatch 200B, Molecular Devices) in voltage clamp mode (that is, at constant applied voltage). (See Supplementary Section S9 for a description of data acquisition methods.) We determined the resistance between electrodes by measuring the current at various applied voltages in the range of ±0.5 V; the slope of the corresponding current versus voltage plots equalled the inverse of the resistance. To measure the resistance as a function of the bilayer thickness, different lipid bilayers were formed on the same chip by using SUVs composed of DLPC, DMPC, DΔPPC or DEPC lipids. This chip was cleaned before the formation of each lipid bilayer as described above. The chip used for these experiments contained a nanopore with a diameter of 28 nm and length of 12 nm (see Supplementary Section S1 for a TEM image) and the recording buffer contained 500 mM KCl and 10 mM HEPES at a pH of 7.4±0.1. To measure the resistance of nanopores as a function of temperature, we used a feedback-controlled Peltier Cooler from Warner Instruments (Supplementary Section S1).

Sensing proteins with biotinylated lipids in the bilayer. Supported lipid bilayers were formed on the silicon chip from SUVs containing 0.15–0.4 mol% biotin-PE, 0.8 mol% Rh-PE and ~99 mol% POPC. We used an electrolyte containing 2.0 M KCl and 10 mM HEPES with a pH of 7.4±0.1 and performed all current recordings at −0.1 V. To detect SA, we used a nanopore with an area-equivalent diameter of 19.2 nm (Supplementary Section S1) and a length of 18 nm (before formation of the bilayer), and added streptavidin to the top compartment at concentrations of 3.2–6.2 pM. To detect mAb and Fab, we used a nanopore with an area-equivalent diameter of 33.0 nm and a length of 22 nm; we added mAb or Fab to the top compartment at concentrations of mAb or Fab of 0.1–50 nM. (See Supplementary Section S9 for a description of the resistive-pulse analysis.)

Detection of aggregates of Aβ peptides. See Supplementary Section S10 for a description of Aβ sample preparation. We used a nanopore with a diameter of 96 nm and a length of ~275 nm (before bilayer coating), which was either uncoated or coated with a POPC bilayer. Solutions containing Aβ peptides (residues 1–40) were added to the top compartment at Aβ concentrations of 0.1–0.2 mg ml^{-1}. We used a recording electrolyte containing 70 mM KCl and 10 mM HEPES with a pH of 7.4±0.1 and recorded resistive pulses at +0.2 V.

Received 28 July 2010; accepted 17 January 2011; published online 20 February 2011

References

1. Sexton, L. T. *et al.* Resistive-pulse studies of proteins and protein/antibody complexes using a conical nanotube sensor. *J. Am. Chem. Soc.* **129,** 13144–13152 (2007).
2. Movileanu, L., Howorka, S., Braha, O. & Bayley, H. Detecting protein analytes that modulate transmembrane movement of a polymer chain within a single protein pore. *Nature Biotechnol.* **18,** 1091–1095 (2000).
3. Howorka, S. & Siwy, Z. Nanopore analytics: sensing of single molecules. *Chem. Soc. Rev.* **38,** 2360–2384 (2009).
4. Siwy, Z. *et al.* Protein biosensors based on biofunctionalized conical gold nanotubes. *J. Am. Chem. Soc.* **127,** 5000–5001 (2005).
5. Ding, S., Gao, C. L. & Gu, L. Q. Capturing single molecules of immunoglobulin and ricin with an aptamer-encoded glass nanopore. *Anal. Chem.* **81,** 6649–6655 (2009).
6. Uram, J. D., Ke, K., Hunt, A. J. & Mayer, M. Submicrometer pore-based characterization and quantification of antibody–virus interactions. *Small* **2,** 967–972 (2006).
7. Branton, D. *et al.* The potential and challenges of nanopore sequencing. *Nature Biotechnol.* **26,** 1146–1153 (2008).
8. Iqbal, S. M., Akin, D. & Bashir, R. Solid-state nanopore channels with DNA selectivity. *Nature Nanotech.* **2,** 243–248 (2007).
9. Wanunu, M., Morrison, W., Rabin, Y., Grosberg, A. Y. & Meller, A. Electrostatic focusing of unlabelled DNA into nanoscale pores using a salt gradient. *Nature Nanotech.* **5,** 160–165 (2010).
10. Uram, J. D., Ke, K., Hunt, A. J. & Mayer, M. Label-free affinity assays by rapid detection of immune complexes in submicrometer pores. *Angew. Chem. Int. Ed.* **45,** 2281–2285 (2006).
11. Robertson, J. W. F. *et al.* Single-molecule mass spectrometry in solution using a solitary nanopore. *Proc. Natl Acad. Sci. USA* **104,** 8207–8211 (2007).
12. Han, A. P. *et al.* Label-free detection of single protein molecules and protein-protein interactions using synthetic nanopores. *Anal. Chem.* **80,** 4651–4658 (2008).
13. Ito, T., Sun, L. & Crooks, R. M. Simultaneous determination of the size and surface charge of individual nanoparticles using a carbon nanotube-based Coulter counter. *Anal. Chem.* **75,** 2399–2406 (2003).
14. Talaga, D. S. & Li, J. L. Single-molecule protein unfolding in solid state nanopores. *J. Am. Chem. Soc.* **131,** 9287–9297 (2009).
15. Oukhaled, G. *et al.* Unfolding of proteins and long transient conformations detected by single nanopore recording. *Phys. Rev. Lett.* **98,** 158101 (2007).
16. Benner, S. *et al.* Sequence-specific detection of individual DNA polymerase complexes in real time using a nanopore. *Nature Nanotech.* **2,** 718–724 (2007).
17. Clarke, J. *et al.* Continuous base identification for single-molecule nanopore DNA sequencing. *Nature Nanotech.* **4,** 265–270 (2009).
18. Bayley, H. & Cremer, P. S. Stochastic sensors inspired by biology. *Nature* **413,** 226–230 (2001).
19. Nakane, J. J., Akeson, M. & Marziali, A. Nanopore sensors for nucleic acid analysis. *J. Phys. Condens. Matter* **15,** R1365–R1393 (2003).
20. Dekker, C. Solid-state nanopores. *Nature Nanotech.* **2,** 209–215 (2007).
21. Martin, C. R. & Siwy, Z. S. Learning nature's way: biosensing with synthetic nanopores. *Science* **317,** 331–332 (2007).
22. Movileanu, L. Interrogating single proteins through nanopores: challenges and opportunities. *Trends Biotechnol.* **27,** 333–341 (2009).
23. Majd, S. *et al.* Applications of biological pores in nanomedicine, sensing, and nanoelectronics. *Curr. Opin. Biotechnol.* **21,** 439–476 (2010).
24. Hou, X. *et al.* A biomimetic potassium responsive nanochannel: G-Quadruplex DNA conformational switching in a synthetic nanopore. *J. Am. Chem. Soc.* **131,** 7800–7805 (2009).
25. Yameen, B. *et al.* Single conical nanopores displaying pH-tunable rectifying characteristics. Manipulating ionic transport with zwitterionic polymer brushes. *J. Am. Chem. Soc.* **131,** 2070–2071 (2009).
26. Sexton, L. T. *et al.* An adsorption-based model for pulse duration in resistive-pulse protein sensing. *J. Am. Chem. Soc.* **132,** 6755–6763 (2010).
27. Pedone, D., Firnkes, M. & Rant, U. Data analysis of translocation events in nanopore experiments. *Anal. Chem.* **81,** 9689–9694 (2009).
28. Uram, J. D., Ke, K. & Mayer, M. Noise and bandwidth of current recordings from submicrometer pores and nanopores. *ACS Nano* **2,** 857–872 (2008).
29. Fologea, D., Ledden, B., David, S. M. & Li, J. Electrical characterization of protein molecules by a solid-state nanopore. *Appl. Phys. Lett.* **91,** 053901 (2007).
30. Chun, K. Y., Mafe, S., Ramirez, P. & Stroeve, P. Protein transport through gold-coated, charged nanopores: effects of applied voltage. *Chem. Phys. Lett.* **418,** 561–564 (2006).

31. Hille, B. *Ion Channels of Excitable Membranes* (Sinauer Associaties, 2001).
32. Steinbrecht, R. A. Pore structures in insect olfactory sensilla: a review of data and concepts. *Int. J. Insect Morphol. Embryol.* **26,** 229–245 (1997).
33. Zacharuk, R. Y. Antennae and sensilla, in *Comparative Insect Physiology Chemistry and Pharmacology* (eds Kerkut, G. A. & Gilbert, L. I.) (Pergamon Press, 1985).
34. Locke, M. Permeability of insect cuticle to water and lipids. *Science* **147,** 295–298 (1965).
35. Nilsson, J., Lee, J. R. I., Ratto, T. V. & Letant, S. E. Localized functionalization of single nanopores. *Adv. Mater.* **18,** 427–431 (2006).
36. Wang, G. L., Zhang, B., Wayment, J. R., Harris, J. M. & White, H. S. Electrostatic-gated transport in chemically modified glass nanopore electrodes. *J. Am. Chem. Soc.* **128,** 7679–7686 (2006).
37. Wanunu, M. & Meller, A. Chemically modified solid-state nanopores. *Nano Lett.* **7,** 1580–1585 (2007).
38. Watts, T. H., Brian, A. A., Kappler, J. W., Marrack, P. & McConnell, H. M. Antigen presentation by supported planar membranes containing affinity-purified I-A^d. *Proc. Natl Acad. Sci. USA* **81,** 7564–7568 (1984).
39. Cremer, P. S. & Boxer, S. G. Formation and spreading of lipid bilayers on planar glass supports. *J. Phys. Chem. B* **103,** 2554–2559 (1999).
40. Reimhult, E., Hook, F. & Kasemo, B. Intact vesicle adsorption and supported biomembrane formation from vesicles in solution: influence of surface chemistry, vesicle size, temperature, and osmotic pressure. *Langmuir* **19,** 1681–1691 (2003).
41. Sackmann, E. Supported membranes: scientific and practical applications. *Science* **271,** 43–48 (1996).
42. Miller, C. E., Majewski, J., Gog, T. & Kuhl, T. L. Characterization of biological thin films at the solid–liquid interface by X-ray reflectivity. *Phys. Rev. Lett.* **94,** 238104 (2005).
43. Bayerl, T. M. & Bloom, M. Physical properties of single phospholipid bilayers adsorbed to micro glass beads—a new vesicular model system studied by ^{2}H nuclear magnetic resonance. *Biophys. J.* **58,** 357–362 (1990).
44. Caffrey, M. & Hogan, J. LIPIDAT: a database of lipid phase transition temperatures and enthalpy changes. DMPC data subset analysis. *Chem. Phys. Lipids* **61,** 1–109 (1992).
45. Tokumasu, F., Jin, A. J. & Dvorak, J. A. Lipid membrane phase behaviour elucidated in real time by controlled environment atomic force microscopy. *J. Electron Microsc.* **51,** 1–9 (2002).
46. Schuy, S. & Janshoff, A. Thermal expansion of microstructured DMPC bilayers quantified by temperature-controlled atomic force microscopy. *ChemPhysChem* **7,** 1207–1210 (2006).
47. Gibbs, A. G. Lipid melting and cuticular permeability: new insights into an old problem. *J. Insect Physiol.* **48,** 391–400 (2002).
48. Adam, G. & Delbrueck, M. Reduction of dimensionality in biological diffusion processes, in *Structural Chemistry and Molecular Biology* (eds Rich, A. & Davidson, N.) 198–215 (W. H. Freeman and Co., 1968).
49. Gambin, Y. *et al.* Lateral mobility of proteins in liquid membranes revisited. *Proc. Natl Acad. Sci. USA* **103,** 2098–2102 (2006).
50. Grover, N. B., Naaman, J., Ben-sasson, S., Doljansk, F. & Nadav, E. Electrical sizing of particles in suspensions. 2. Experiments with rigid spheres. *Biophys. J.* **9,** 1415–1425 (1969).
51. Grover, N. B., Naaman, J., Ben-sasson, S. & Doljansk, F. Electrical sizing of particles in suspensions. I.Theory. *Biophys. J.* **9,** 1398–1414 (1969).
52. Neish, C. S., Martin, I. L., Henderson, R. M. & Edwardson, J. M. Direct visualization of ligand–protein interactions using atomic force microscopy. *Br. J. Pharmacol.* **135,** 1943–1950 (2002).
53. Janeway, C. A. *Immunobiology: The Immune System in Health and Disease* 5th edn (Garland Publishing, 2001).
54. Schneider, S. W., Larmer, J., Henderson, R. M. & Oberleithner, H. Molecular weights of individual proteins correlate with molecular volumes measured by atomic force microscopy. *Pflugers Arch.* **435,** 362–367 (1998).
55. Sivasankar, S., Subramaniam, S. & Leckband, D. Direct molecular level measurements of the electrostatic properties of a protein surface. *Proc. Natl Acad. Sci. USA* **95,** 12961–12966 (1998).
56. Majd, S. & Mayer, M. Hydrogel stamping of arrays of supported lipid bilayers with various lipid compositions for the screening of drug–membrane and protein–membrane interactions. *Angew. Chem. Int. Ed.* **44,** 6697–6700 (2005).
57. Capone, R. *et al.* Amyloid-beta-induced ion flux in artificial lipid bilayers and neuronal cells: resolving a controversy. *Neurotox. Res.* **16,** 1–13 (2009).
58. Li, J. *et al.* Ion-beam sculpting at nanometre length scales. *Nature* **412,** 166–169 (2001).
59. Lewis, B. A. & Engelman, D. M. Lipid bilayer thickness varies linearly with acyl chain-length in fluid phosphatidylcholine vesicles. *J. Mol. Biol.* **166,** 211–217 (1983).

Acknowledgements

The authors thank D. Sept and D. Talaga for assistance in modelling distributions of translocation times and Y.N. Billeh for valuable discussions. The authors also thank D.J. Estes and J.D. Uram for their work on the LabView recording software. This work was supported by a National Science Foundation Career Award (M.M., grant no. 0449088), the National Institutes of Health (M.M., grant no. 1R01GM081705), the Alzheimer's Disease Research Center (J.Y., 3P50 AG005131), the Alzheimer's Association (J.Y., NIRG-08-91651), the National Human Genome Research Institute (J.L., grant nos HG003290 and HG004776) and a Graduate Assistance in Areas of National Need Fellowship (E.C.Y).

Author contributions

E.C.Y., J.Y., and M.M. conceived and designed the experiments. E.C.Y., J.M.J., S.M. and P.P. performed the experiments. R.C.R. and J.L. fabricated the nanopores. E.C.Y., J.L., J.Y. and M.M. co-wrote the manuscript and Supplementary Information.

Additional information

The authors declare no competing financial interests. Supplementary information accompanies this paper at www.nature.com/naturenanotechnology. Reprints and permission information is available online at http://npg.nature.com/reprintsandpermissions/. Correspondence and requests for materials should be addressed to J.Y. and M.M.